Journal of Biomedical Optics

SPIEDigitalLibrary.org/jbo

Photoacoustic microscopy of microvascular responses to cortical electrical stimulation

Vassiliy Tsytsarev
Song Hu
Junjie Yao
Konstantin Maslov
Dennis L. Barbour
Lihong V. Wang

Photoacoustic microscopy of microvascular responses to cortical electrical stimulation

Vassiliy Tsytsarev,[a,b,*] Song Hu,[a,*] Junjie Yao,[a] Konstantin Maslov,[a] Dennis L. Barbour,[a] and Lihong V. Wang[a]
[a]Washington University in St. Louis, Department of Biomedical Engineering, One Brookings Drive, St. Louis, Missouri 63130
[b]George Mason University, Krasnow Institute for Advanced Study, Molecular Neuroscience Department, 4400 University Drive, Fairfax, Virginia 22030

Abstract. Advances in the functional imaging of cortical hemodynamics have greatly facilitated the understanding of neurovascular coupling. In this study, label-free optical-resolution photoacoustic microscopy (OR-PAM) was used to monitor microvascular responses to direct electrical stimulations of the mouse somatosensory cortex through a cranial opening. The responses appeared in two forms: vasoconstriction and vasodilatation. The transition between these two forms of response was observed in single vessels by varying the stimulation intensity. Marked correlation was found between the current-dependent responses of two daughter vessels bifurcating from the same parent vessel. Statistical analysis of twenty-seven vessels from three different animals further characterized the spatial-temporal features and the current dependence of the microvascular response. Our results demonstrate that OR-PAM is a valuable tool to study neurovascular coupling at the microscopic level. [DOI: 10.1117/1.3594785]

Keywords: neurovascular coupling; electrical stimulation; vasoconstriction; vasodilatation; optical-resolution photoacoustic microscopy.

Paper 10570RR received Oct. 21, 2010; revised manuscript received Apr. 4, 2011; accepted for publication May 5, 2011; published online Jul. 1, 2011.

1 Introduction

Neurovascular coupling links local neural activities with spatial-temporal changes in cerebral hemodynamics; including total hemoglobin concentration (HbT), hemoglobin oxygen saturation (sO_2), and blood flow.[1,2] This feature has been widely utilized by functional brain imaging techniques [such as magnetic resonance imaging (MRI), diffuse optical tomography (DOT), and photoacoustic tomography (PAT)] as a minimally invasive or noninvasive method to infer brain function.[3–6]

However, exploring the mechanism of neurovascular coupling at the microscopic level remains challenging. Clinical neuroimaging modalities (such as MRI and DOT) lack the spatial resolution for microvascular imaging,[7] and high-resolution purely optical microscopy techniques (such as fluorescence microscopy and optical coherence tomography) have limited access to hemodynamic parameters, especially sO_2.[8] PAT has the potential to overcome these limitations by enabling label-free quantification of cerebral hemodynamic changes in HbT, sO_2, and blood flow velocity at various spatial scales.[9] As a first-in-kind neurovascular study using photoacoustics, Wang et al. used photoacoustic computed tomography (PACT) to observe the hemodynamic response of somatosensory cortex to mechanical stimulation of the rat whisker pad.[6] Providing a spatial resolution comparable to clinical modalities (200 μm), the early-version PACT was not able to image the microvasculature itself. Later with acoustic-resolution photoacoustic microscopy (AR-PAM), Stein et al. demonstrated hemodynamic monitoring of individual vessels under hypoxic and hyperoxic challenges.[10] Although having a much refined resolution (70 μm laterally), AR-PAM still has difficulty in resolving distal microvessels and single capillaries, which are assumed to have the closest spatial correlation with neural activities.[11] Recently, Maslov et al. developed optical-resolution photoacoustic microscopy (OR-PAM).[12] With diffraction-limited optical focusing, OR-PAM enables transcranial imaging of murine cerebral microvascular morphology and oxygenation at the resolution of individual capillaries.[13,14] Quantitative monitoring of microhemodynamics, such as vasodilatation, vasomotion, and changes in blood flow, has also been documented with this technique.[15,16]

In this work, OR-PAM was used for the first time to explore neurovascular coupling at the microscopic level in a cortical electrical stimulation model. Direct electrical stimulation may cause cortical neurons to generate action potentials and synaptic release of various neurotransmitters, which can further react with nearby astrocytes, smooth muscle cells, and endothelial cells of the vessel wall.[1] The net effect of these reactions drives cortical vessels from the resting state to either vasoconstriction or vasodilatation. Alternatively, smooth muscle cells and astrocytes can directly respond to electrical stimulation:[17] direct electrical stimulation of smooth muscle cells may cause vasoconstriction, while direct electrical stimulation of astrocytes may result in intracellular calcium waves along the astrocytic syncytium, which may signal the release of various neuromodulators to direct blood vessels to regulate the metabolic supply by increasing or decreasing the local vessel capacity.[18,19] Moreover, electrical stimulation of brain tissue temporarily increases extracellular potassium concentration, which can potentially cause neural

*The authors contributed equally to this work.

Address correspondence to: Lihong V. Wang, Washington University in St. Louis, Department of Biomedical Engineering, Optical Imaging Laboratory, One Brookings Drive, St. Louis, Missouri 63130-4899. Tel: 314-935-6152; Fax: 314-935-7448; E-mail: lhwang@biomed.wustl.edu.

1083-3668/2011/16(7)/076002/6/$25.00 © 2011 SPIE

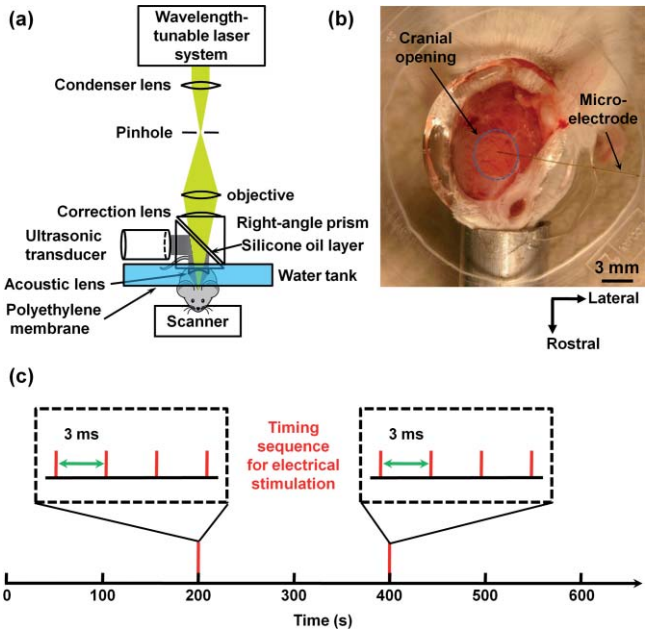

Fig. 1 (a) Schematic of the optical-resolution photoacoustic microscope. (b) Photograph of the exposed mouse brain surface with an introduced microelectrode. (c) Timing sequence for electrical stimulation.

hyperactivity. Increased neural activity requires more blood flow, which may result in vasodilatation.[1,19] Using OR-PAM, we observed both vasodilatation and vasoconstriction in response to cortical electrical stimulation. We further studied the electrical current dependence and the spatial-temporal characteristics of these two types of microvascular responses, at both single-vessel and statistical (27 vessels in total) levels. The results indicate that OR-PAM provides sufficient spatial resolution and adequate temporal resolution to study the coupling between neural activities and individual cortical microvessels.

2 Materials and Methods

Experiments were performed on three animals using our reflection-mode OR-PAM system [Fig. 1(a)]. In our OR-PAM system, a dye laser pumped by an Nd:YLF laser is used as the wavelength-tunable irradiation source. Laser beam from the dye laser is focused by a condenser lens and then spatially filtered by a 25-μm diameter pinhole. A microscope objective then images the pinhole to a near-diffraction-limited focal spot into the brain cortex. An acoustic-optical beam splitter, consisting of two right-angle prisms and a thin layer of silicone oil, is located under the objective to separate optical illumination and acoustic detection. A 75-MHz ultrasonic transducer is attached to the vertical side of the bottom prism. An acoustic lens is attached to the bottom of the splitter and immersed in the water tank to collect photoacoustic signals. Two-dimensional raster scanning along the transverse plane, in combination with time-resolved ultrasonic detection along the depth direction, records complete volumetric information. The detailed system configuration has been previously described.[12,13]

A mouse cerebral cortex consists of six layers of histologically and functionally distinct neurons and glial cells. The thickness of an adult mouse cortex is usually within 1 mm and the cortical surface is covered by dura mater. In the present study, our stimulation targets on the somatosensory cortex. Before each experiment, a Swiss Webster mouse (Hsd: ND4, 25 to 30 g; Harlan, Indianapolis, Indiana) was anesthetized by intraperitoneally administering a dose of 87 mg/kg ketamine and 13 mg/kg xylazine. The animal was placed into a custom-made stereotaxic imaging stage, and the left dorsal portion of the skull was exposed by removing the scalp and temporal muscle. A cranial opening ($\sim$4$\times$4 mm^2) was made using a dental drill over the left somatosensory cortex, and the exposed dura mater surface was cleaned with artificial cerebrospinal fluid. A monopolar tungsten electrode (impedance: 1 MΩ; tip diameter: 10 μm; MicroProbes for Life Science, Gaithersburg, Maryland) was introduced into the cortex to a depth of 0.1 to 0.2 mm through the opening at about 2 mm lateral to sagittal suture and 2 mm posterior to bregma to induce the preset electrical stimulation [Figs. 1(b) and 1(c)]. The teeth-holder of the stereotaxic stage was used as a reference electrode. Anesthesia was maintained using vaporized 1.0% isoflurane with an air flow rate of 1.0 L/min. The body temperature of the animal was kept at 37°C by a temperature-controlled heating pad.

For effective acoustic coupling, the OR-PAM imaging head was submerged in a custom-made water tank, where an imaging window was opened in the bottom of a Petri dish and was sealed with an ultrasonically and optically transparent polyethylene membrane. Ultrasonic gel (Clear Image, SonoTech) between the polyethylene membrane and the brain surface coupled the generated photoacoustic wave from the brain to the water tank, and deionized water inside the tank further coupled the wave to the imaging head. To mitigate possible disturbance to the brain, a drop of saline was placed on the dura mater before applying ultrasonic gel. To eliminate the possible mechanical oscillation of the open brain, the polyethylene membrane in the bottom of the water tank gently pressed against the dura mater.

During each experiment, we first used an isosbestic wavelength of 570 nm to image the vascular system structure in a 2$\times$2 mm^2 cortical region through the cranial opening (Fig. 2, gray scale). Then, within a smaller region of interest around the tip of the microelectrode, wavelengths of 570 and 578 nm were used to quantify sO_2.[12,15] The overlaid structural and sO_2 (functional) images are shown in Fig. 2. Upon observing the vascular system structure and sO_2 distribution, we randomly selected a cross-sectional scan (B-scan) crossing both arterioles and venules (indicated by the dashed line in Fig. 2) for hemodynamic monitoring with various stimulation intensities. Each monitoring trial lasted for 600 s (300 B-scans at 570 nm), during which two identical electrical stimulation sequences were executed 200 and 400 s after the first B-scan, respectively [Fig. 1(c)]. Each stimulus consisted of a train of four identical square pulses (pulse duration: 0.3 ms; repetition rate: 300 Hz; current intensity: 100 to 400 μA) generated by a stimulator (A365; World Precision Instruments, Sarasota, Florida) triggered by a function generator (DS345; Stanford Research Systems, Sunnyvale, California). The time interval between two adjacent trials was 10 min.

After image acquisition, photoacoustic amplitudes were extracted via the Hilbert transformation using the "hilbert" function in MATLAB (MathWorks, Natick, Massachusetts). To distinguish vessels from background, we empirically set the amplitude threshold to be 3 dB above the noise level, which was

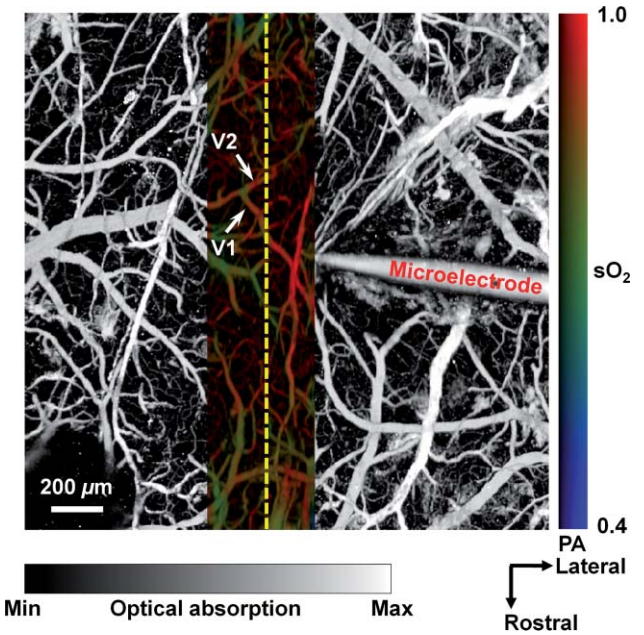

Fig. 2 Superimposed open-skull photoacoustic images of the mouse cortical microvasculature. The maximum-amplitude projection image acquired at 570 nm is shown in gray scale, and the vessel-by-vessel hemoglobin oxygen saturation mapping of a smaller region calculated from dual-wavelength measurements is shown in color scale. B-scan monitoring of the vascular response was performed along the yellow dashed line. V1 and V2 are the two microvessels studied in Fig. 3. (Color online only.)

defined as the standard deviation of the background noise amplitude. After converting the photoacoustic image into a binary image using the amplitude threshold, the cross section of each vessel was identified (i.e., segmentation) by 8-connected labeling using the Image Processing Toolbox in MATLAB. Because the transverse resolution of OR-PAM (5 μm) is much finer than the axial resolution (15 μm) and thus provides more accurate measurements, the vessel diameter was calculated along the transverse direction. The initial condition (baseline) was defined as the mean value of the vessel diameter before the first stimulation in each trial. To compensate for the slow baseline drift and the oblique angle subtended by the B-scan direction and the vessel axis, the time course of the vessel diameter was normalized to its baseline at each trial. Changes in vessel diameter were also normalized to the baseline. The duration of vasodilatation was defined as the period during which the vessel remained a response (in diameter) that is above 90% of the maximum response. The response time was defined as the period during which the vessel response monotonically changed from 10 to 90% of the maximum response; similarly, the recovery time was defined as the period during which the vessel response monotonically changed from 90 to 10% of the maximum response.

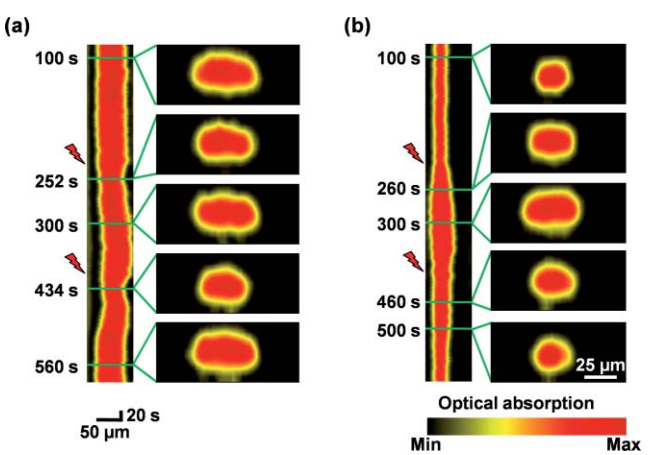

Fig. 3 B-scan monitoring of vasoconstriction and vasodilatation induced by direct electrical stimulations at (a) 100 and (b) 150 μA (B-scan rate is 0.5 Hz). In each panel, the left column is the time course of the change in vessel diameter (represented by the projection of the vessel cross section). The right column is the vessel cross-sectional image at different time points, indicated by the green lines. The red lightning symbol indicates the onset of the stimulation. (Color online only.)

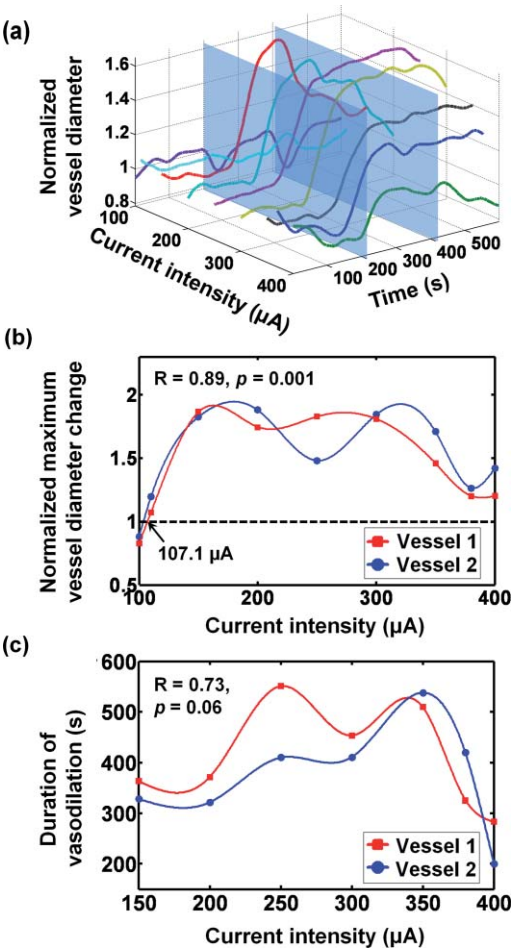

Fig. 4 Current-dependent vascular response studied in individual microvessels. (a) Time courses of the diameter change in V1 under various stimulation intensities. (b) and (c) Correlation of the current-dependent vascular responses of two daughter vessels (V1 and V2) bifurcated from the same parent vessel: (b) normalized maximum diameter change and (c) the duration of vasodilatation. The two semi-transparent planes in panel (a) indicate the time points of the two stimuli. (Color online only.)

After each experiment, the animal was euthanized with an overdose of pentobarbital. All experimental animal procedures were carried out in conformance with the laboratory animal protocol approved by the School of Medicine Animal Studies Committee of Washington University in St. Louis.

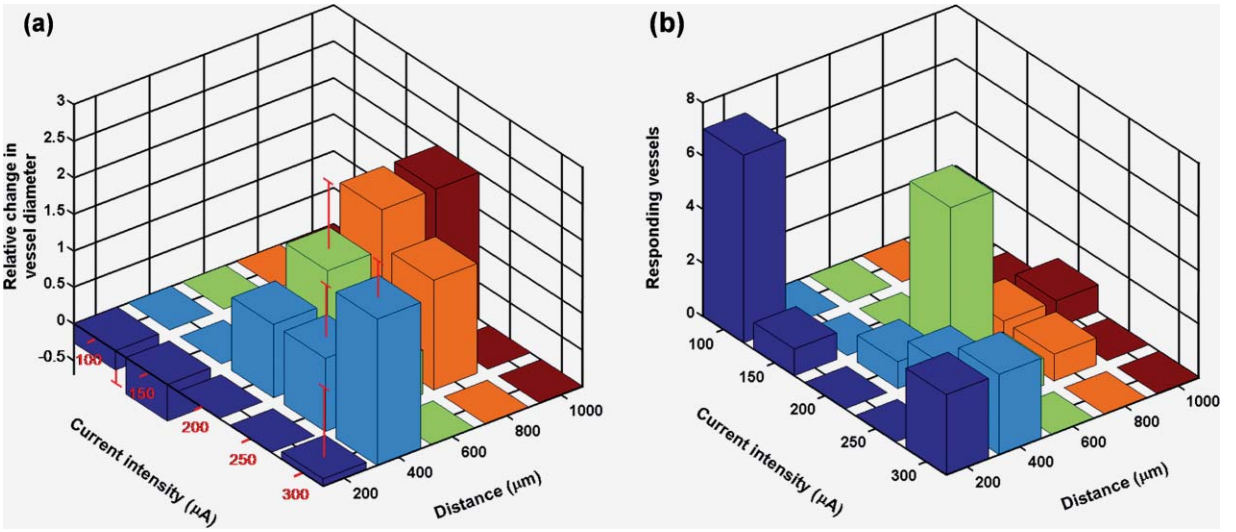

Fig. 5 Spatial characteristics of vasoconstriction and vasodilatation at different stimulation currents studied in 27 microvessels. (a) Relative change in vessel diameter versus distance from the electrode tip. (b) Number of responding vessels versus distance from the electrode tip. For clarification, the relative diameter changes and the numbers of responding vessels are listed in 1(a) and 1(b), respectively.

3 Results

OR-PAM provides high spatial resolution, adequate temporal resolution, and a large field of view (FOV),[13,15] allowing us to simultaneously study the responses of individual vessels at different spatial locations. The present study investigated a total of 30 microvessels within 1 mm of the stimulating electrode from three different animals. In response to intracortical electrical stimulation, nine vessels showed only vasoconstriction, 15 showed only vasodilatation, three showed both, and the remaining three showed no response.

Figure 3 demonstrates the vasoconstriction and vasodilatation of the same microvessel (V1 in Fig. 2) in response to electrical stimulations at different current levels. At 100 μA, a distinct vasoconstriction appeared after each of the two stimuli [Fig. 3(a)]. At 150 μA, the first stimulus produced a pronounced and prolonged vasodilatation, which prevented the vessel from recovering back to the resting state before the arrival of the second stimulus [Fig. 3(b) and Video 1]. Changes in vessel diameter were not clearly observed in the axial direction because the axial resolution (15 μm) of OR-PAM was not adequate to resolve such small changes. Note that the baseline diameters of the microvessel (defined as the average transverse dimension of the vessel prior to the first stimulation in each monitoring trial) were different between the two trials [the left panels in Figs. 3(a) and 3(b)], possibly due to the isoflurane anesthesia and the open-skull condition.[20] Also note that the vessel cross sections in Fig. 3 appeared elliptic because the B-scan crossed the vessel at an oblique angle rather than a right angle. However, by normalization on initial condition, the influence of these two effects on the quantification of relative changes in vessel diameter can be eliminated.

Figure 4(a) further shows the current-dependent response of microvessel V1. At 100 μA [purple curve in Fig. 4(a)], a rapid vasoconstriction was induced right after each stimulus, with as much as an 18% decrease in vessel diameter; however, higher stimulation currents (from 110 up to 400 μA) led to a transition from rapid vasoconstriction to prolonged vasodilatation, with a diameter increase of as high as 87%. The normalized maximum diameter changes of V1 at a variety of stimulation currents were plotted in Fig. 4(b) (red squares) and fitted with the smoothing spline function (red curve) in MATLAB.

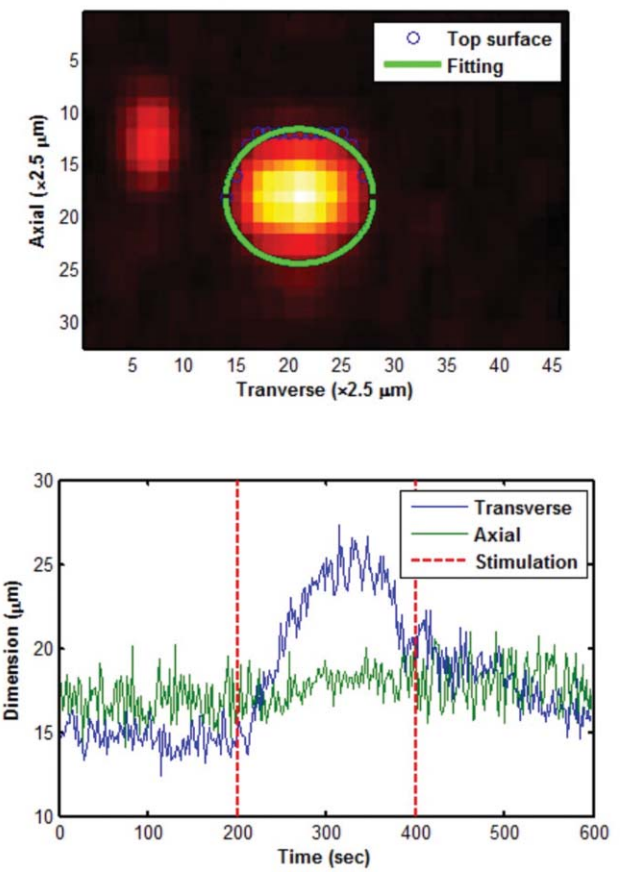

Video 1 Vascular response in individual microvessel. (QuickTime, 9.9 MB) [URL: http://dx.doi.org/10.1117/1.3594785.1]

Table 1 Spatial characteristics of vasoconstriction and vasodilatation at different stimulation currents studied in 27 microvessels.

(a) Relative change in vessel diameter versus distance from the electrode tip. Values are in mean ± standard deviation format.

Current (μA) \ Distance (μm)	200	400	600	800	1000
100	-0.26 ± 0.48	0	0	0	0
150	-0.50	0	0	0	0
200	0	1.00	1.45 ± 0.92	2.00	2.00
250	0	1.00 ± 0.71	0.60	1.50	0
300	0.10 ± 0.95	2.00 ± 0.50	0	0	0

(b) Number of responding vessels versus distance from the electrode tip.

Current (μA) \ Distance (μm)	200	400	600	800	1000
100	7	0	0	0	0
150	1	0	0	0	0
200	0	1	6	1	1
250	0	2	1	1	0
300	3	3	0	0	0

According to the fitting curve, the critical stimulation intensity corresponding to the transition from vasoconstriction to vasodilatation was estimated to be ~107 μA. Besides the transition in vascular response, the amplitude and the duration of vasodilatation of V1 were found to be nonmonotonic with the current intensity [red curves in Figs. 4(b) and 4(c)]. This nonmonotonic response likely suggests both coexistence and competition between vasoconstriction and vasodilatation. Interestingly, the other daughter vessel (V2 in Fig. 2), which bifurcated from the same parent vessel as V1, showed very similar responses [blue curves in Figs. 4(b) and 4(c)]. The Pearson correlation coefficients of the current-dependent vasodilatation amplitude and duration were calculated to be 0.89 ($p = 0.001$) and 0.73 ($p = 0.06$), respectively, using the standard function "corrcoef" in MATLAB.

OR-PAM's large FOV enabled exploration of the spatial features of the microvascular response. All 27 microvessels that showed responses in the three experiments were studied in this way [Fig. 5 and Table 1]. When microvessels were within 300 μm of the electrode tip, there was a clear transition from vasoconstriction to vasodilatation with increased stimulation intensity [blue bars in Fig. 5(a) and Table 1(a)]. Throughout this transition, both the response amplitude and the number of responding vessels were diminished, suggesting a transition in the balance between vasoconstriction and vasodilatation [blue bars in Figs. 5(a) and 5(b)]. However, in vessels that were farther from the electrode tip (>300 μm), vasodilatation became more dominant. Another observation was that the total number of responsive vessels decreased with increased distance from the electrode tip, which likely reflected the decay of stimulation intensity due to the radial current diffusion [Fig. 5(b) and Table 1(b)].

The temporal features of vasodilatation and vasoconstriction were further statistically studied, as shown in Fig. 6 (nine vessels for vasoconstriction and 15 vessels for vasodilatation). For each vessel, vasoconstriction or vasodilatation occurring at the lowest stimulation current was chosen for study. The unpaired 1-tailed Wilcoxon signed rank test showed that the response and recovery times of vasodilatation were significantly longer than those of vasoconstriction. Interestingly, although both the response phase of vasodilation and the recovery phase of vasoconstriction represent the increase in vessel diameter, their time scales are quite different (the same situation for the recovery phase of vasodilation and the response phase of

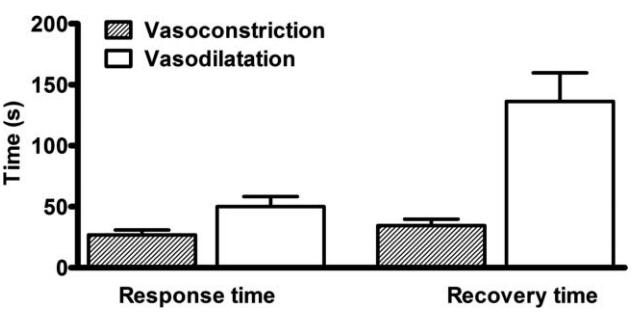

Fig. 6 Temporal characteristics of vasoconstriction (nine vessels) and vasodilatation (15 vessels). The response (rising/falling) time and recovery time of vasodilatation are compared with those of vasoconstriction, using the 1-tailed Wilcoxon signed rank test. The response and recovery times of vasodilatation are statistically significantly longer than those of vasoconstriction (p values for both response and recovery cases are 0.005).

vasoconstriction). This suggests the different underlying mechanisms of the two types of vascular response.

4 Discussion

Responses of individual microvessels in a mouse cortex to intracortical electrical stimulation were studied with OR-PAM. The relatively small fluctuation ($\pm 10\%$) in the baseline vessel diameter during each OR-PAM monitoring suggested that the neurovascular system remained at a resting state under consistent physiological conditions (Fig. 4). However, this balance could be perturbed by electrical-stimulation-induced vasoconstriction or vasodilatation, depending on stimulation intensity and other factors.

Both the dual reaction of some vessels to electrical stimulation and the pronounced difference in the temporal features of the two types of neurovascular response suggest that vasoconstriction and vasodilatation result from different cellular regulations, which is consistent with previous findings.[18] One possible explanation is that vasoconstriction, likely caused by direct electrical stimulation of smooth muscle cells, is related to mechanical features of vessel walls and can take place in a short time,[2,21] while vasodilatation, possibly caused by the various neurotransmitters and neuromodulators, may take longer because of the relatively slow transmission speed of neuromodulator signals. However, more carefully designed experiments are required to further reveal the underlying mechanisms.

In summary, label-free OR-PAM was used to the spatial-temporal characteristics and current dependence of the microvascular response to cortical electrical stimulation. The high spatial resolution enables analyzing single vessel responses, and the large FOV allows simultaneous imaging of multiple microvessels for studying correlation and performing statistical analysis. OR-PAM is a promising tool for *in vivo* studies of neurovascular coupling at the microscopic level.

Acknowledgments

The authors thank Christopher Favazza and Arie Krumholz for helpful discussions, Dr. Alexey Glukhov for technical support, and Professor James Ballard, Dr. Lynnea Brumbaugh, and Ms. Kristy Wendt for help in editing the manuscript. This work was supported by National Institutes of Health Grants Nos. R01 EB000712, EB000712A2S1, R01 EB00071207S2, R01 EB008085, R01 CA113453901, U54 CA136398, and 5P60 DK02057933. L.W. has a financial interest in Microphotoacoustics, Inc. and Endra, Inc., which, however, did not support this work.

References

1. N. J. Allen and B. A. Barres, "Neuroscience: Glia – more than just brain glue," *Nature* **457**(7230), 675–677 (2009).
2. M. Y. Inyushin, A. B. Vol'nova, and D. N. Lenkov, "Use of a simplified method of optical recording to identify foci of maximal neuron activity in the somatosensory cortex of white rats," *Neurosci. Behav. Physiol.* **31**(2), 201–205 (2001).
3. R. D. Frostig, E. E. Lieke, D. Y. Ts'o, and A. Grinvald, "Cortical functional architecture and local coupling between neuronal activity and the microcirculation revealed by in vivo high-resolution optical imaging of intrinsic signals," *Proc. Natl. Acad. Sci. U.S.A.* **87**(16), 6082–6086 (1990).
4. K. Uludag, D. J. Dubowitz, E. J. Yoder, K. Restom, T. T. Liu, and R. B. Buxton, "Coupling of cerebral blood flow and oxygen consumption during physiological activation and deactivation measured with fMRI," *Neuroimage* **23**(1), 148–155 (2004).
5. J. P. Culver, T. Durduran, D. Furuya, C. Cheung, J. H. Greenberg, and A. G. Yodh, "Diffuse optical tomography of cerebral blood flow, oxygenation, and metabolism in rat during focal ischemia," *J. Cereb. Blood Flow Metab.* **23**(8), 911–924 (2003).
6. X. Wang, Y. Pang, G. Ku, X. Xie, G. Stoica, and L. V. Wang, "Noninvasive laser-induced photoacoustic tomography for structural and functional in vivo imaging of the brain," *Nat. Biotechnol.* **21**(7), 803–806 (2003).
7. S. Hu and L. V. Wang, "Neurovascular photoacoustic tomography," *Front. Neuroenerg.* **2**, 10 (2010).
8. S. Hu and L. V. Wang, "Photoacoustic imaging and characterization of the microvasculature," *J. Biomed. Opt.* **15**(1), 011101 (2010).
9. L. V. Wang, "Multiscale photoacoustic microscopy and computed tomography," *Nat. Photonics* **3**, 503–509 (2009).
10. E. W. Stein, K. Maslov, and L. V. Wang, "Noninvasive, in vivo imaging of blood-oxygenation dynamics within the mouse brain using photoacoustic microscopy," *J. Biomed. Opt.* **14**(2), 020502 (2009).
11. E. M. Hillman, A. Devor, M. B. Bouchard, A. K. Dunn, G. W. Krauss, J. Skoch, B. J. Bacskai, A. M. Dale, and D. A. Boas, "Depth-resolved optical imaging and microscopy of vascular compartment dynamics during somatosensory stimulation," *Neuroimage* **35**(1), 89–104 (2007).
12. K. Maslov, H. F. Zhang, S. Hu, and L. V. Wang, "Optical-resolution photoacoustic microscopy for in vivo imaging of single capillaries," *Opt. Lett.* **33**(9), 929–931 (2008).
13. S. Hu, K. Maslov, V. Tsytsarev, and L. V. Wang, "Functional transcranial brain imaging by optical-resolution photoacoustic microscopy," *J. Biomed. Opt.* **14**(4), 040503 (2009).
14. H. F. Zhang, K. Maslov, M. Sivaramakrishnan, G. Stoica, and L. H. V. Wang, "Imaging of hemoglobin oxygen saturation variations in single vessels in vivo using photoacoustic microscopy," *Appl. Phys. Lett.* **90**(5), 053901 (2007).
15. S. Hu, K. Maslov, and L. V. Wang, "Noninvasive label-free imaging of microhemodynamics by optical-resolution photoacoustic microscopy," *Opt. Express* **17**(9), 7688–7693 (2009).
16. J. J. Yao, K. I. Maslov, Y. F. Shi, L. A. Taber, and L. H. V. Wang, "In vivo photoacoustic imaging of transverse blood flow by using Doppler broadening of bandwidth," *Opt. Lett.* **35**(9), 1419–1421 (2010).
17. V. Tsytsarev, K. Premachandra, D. Takeshita, and S. Bahar, "Imaging cortical electrical stimulation in vivo: fast intrinsic optical signal versus voltage-sensitive dyes," *Opt. Lett.* **33**(9), 1032–1034 (2008).
18. M. R. Metea and E. A. Newman, "Glial cells dilate and constrict blood vessels: a mechanism of neurovascular coupling," *J. Neurosci.* **26**(11), 2862–2870 (2006).
19. M. Zonta, M. C. Angulo, S. Gobbo, B. Rosengarten, K. A. Hossmann, T. Pozzan, and G. Carmignoto, "Neuron-to-astrocyte signaling is central to the dynamic control of brain microcirculation," *Nat. Neurosci.* **6**(1), 43–50 (2003).
20. D. A. Schwinn, R. W. McIntyre, and J. G. Reves, "Isoflurane-induced vasodilation: role of the alpha-adrenergic nervous system," *Anesth. Analg. (Baltimore)* **71**(5), 451–459 (1990).
21. L. Leybaert, "Neurobarrier coupling in the brain: a partner of neurovascular and neurometabolic coupling?," *J. Cereb. Blood Flow Metab.* **25**(1), 2–16 (2005).